



Free decay and excitation of the Chandler wobble: self-consistent estimates of the period and quality factor

Wei Chen¹ · Yifei Chen¹ · Jim Ray² · Jiesi Luo¹ · Jian Cheng Li^{1,3}

Received: 2 September 2022 / Accepted: 16 March 2023 / Published online: 10 April 2023
© The Author(s) 2023

Abstract

The period T_{CW} and quality factor Q_{CW} of the Chandler wobble (CW) as well as polar motion (PM) transfer functions are all determined by the Earth's layered structure, mass distribution, elasticity, rheology and energy dissipation, via the Earth's dynamic figure parameters and complex degree-2 Love numbers. However, most previous studies used geophysical excitations derived from real-valued PM transfer functions to invert for T_{CW} and Q_{CW} , thus leading to results that are not self-consistent. By separating the observed PM into the freely decaying CW and the excited PM, a traverse-based method is proposed to search values of T_{CW} and Q_{CW} that can fit both sides simultaneously, yielding the self-consistent estimates of $T_{CW} = 430.4$ mean solar days and $Q_{CW} = 130$. This implies the degree-2 tidal Love number $k = 0.35011 - 0.00226i$ and load Love number $k' = -0.36090 + 0.00233i$, and the PM transfer functions $T^{NL} = 1.80001 - 0.00692i$ (non-loading) and $T^L = 1.15040 - 0.00023i$ (loading) valid at the Chandler period.

Keywords Earth rotation · Chandler wobble · Quality factor · Love number · Transfer function

1 Introduction

For an Earth model with (an)elastic mantle, fluid outer core and solid inner core, there are four important normal modes of the rotating Earth, namely the Chandler wobble (CW), the free core nutation (FCN), the free inner core nutation (FICN) and the inner core wobble (ICW) (e.g., Mathews et al 1991, 2002). While the FCN plays a significant role in the Earth's nutations, the CW is one of the two dominant oscillations of the Earth's polar motion (PM; the other is the forced annual wobble, or AW).

Without excitations, the CW would decay freely and vanish within only a few decades due to a number of causes, such as mantle an elasticity and oceanic dissipations, etc.

(e.g., Lambeck 1980; Gross 2015a). The free decay is evident as the decrease in the CW amplitude and thus as the energy loss, which can be described by the CW quality factor Q_{CW} . Then the CW frequency σ_{CW} becomes a complex value and can be written as (with T_{CW} being the CW period)

$$\sigma_{CW} = \frac{2\pi}{T_{CW}} \left(1 + \frac{i}{2Q_{CW}} \right) = \frac{2\pi}{T_{CW}} + i \frac{\pi}{D_{CW}},$$
$$D_{CW} = T_{CW} Q_{CW} \quad (1)$$

with its imaginary part accounting for dissipation.

Numerous studies have been dedicated to the determinations of T_{CW} and Q_{CW} . Around three decades ago, the excitation functions were usually considered to be a random Gaussian process at frequencies near the CW frequency, with the estimated T_{CW} being in the range 433.0–434.8 days with uncertainties between ~ 1–3 days, and Q_{CW} in the range 63–179 with uncertainties between 36–1000 (e.g., Jeffreys 1972; Ooe 1978; Wilson and Haubrich 1976; Wilson and Vicente 1980, 1990). Later, Furuya and Chao (1996) and Kuehne et al. (1996) assumed CW to be maintained by atmospheric excitation, and obtained T_{CW} being respectively 433.7 and 439.5 days with uncertainties 1.8 and 2.1 days, and Q_{CW} being respectively 49 and 72 with uncertainty intervals 35–100 and 30–500. Gross (2005) and Seitz et al. (2012)

Jim Ray: Retired.

✉ Wei Chen
wchen@sgg.whu.edu.cn

¹ Hubei LuoJia Laboratory, School of Geodesy and Geomatics, Wuhan University, Wuhan, People's Republic of China

² National Oceanic and Atmospheric Administration, Silver Spring, Maryland, USA

³ Central South University, Changsha, People's Republic of China

further used the atmospheric and oceanic excitations to estimate T_{CW} and Q_{CW} , with values between 429.4–432.98 days and 83–107, respectively. Bizouard (2020) also considered atmospheric and oceanic excitations and obtained T_{CW} in the range [432, 435] days and Q_{CW} in [43, 102]. Based on satellite laser ranging (SLR) and Gravity Recovery and Climate Experiment (GRACE) observations, Nastula and Gross (2015) obtained $T_{CW} = 430.9 \pm 0.7$ solar days and $Q_{CW} = 127$ (56, 255).

Gross (2000), Gross et al. (2003); also see Brzezinski and Nastula 2002) proved that mass redistributions and relative motions in atmosphere and oceans are the main causes exciting the CW against its free decay. Therefore, the observed CW must not be a purely free wobble but rather a free wobble superposed by a forced resonant oscillation. This fact makes the determinations of the period T_{CW} and especially the quality factor Q_{CW} more complicated since the excited part of CW must be removed to obtain a reliable Q_{CW} , which is closely related to the free decay of the CW. Further, as shown in Chen et al. (2013a), both the PM transfer functions (T^L and T^{NL} , used to derive the effective atmospheric and oceanic excitations as explained in Sect. 4) and the complex CW frequency are determined by the Earth’s layered structure, mass distribution, elasticity, rheology and energy dissipation, via the Earth’s dynamic figure parameters and Love numbers (see Sect. 4 for details). That is, once the transfer functions are chosen, the values of T_{CW} and Q_{CW} are also fixed; thus many of the published estimates are not self-consistent. Further, most previous studies used real valued T^L and T^{NL} , implying the adoption of real Love numbers, while real Love numbers will only produce real CW frequency (and thus Q_{CW} is infinite, contrary to their finite Q_{CW} results). To conclude, improved studies are needed to obtain self-consistent estimates of T_{CW} and Q_{CW} .

In this work, we propose a new and self-consistent traverse-based method to search values of T_{CW} and Q_{CW} that can fit both the freely decaying CW and the excited PM simultaneously, and further provided values of degree-2 complex Love numbers and PM transfer functions valid at the CW frequency.

2 Method

As discussed in the Appendix, the observed time series of PM, since the time t_0 , can be decomposed as

$$p_{\text{obs}}(t) = p_{\text{CW}}^{\text{fd}}(t) + p_{\text{obs}}^{\text{ext}}(t), \tag{2}$$

with the freely decaying part of the CW (let $A_{\text{CW}}^{t_0}$ and $\alpha_{\text{CW}}^{t_0}$ be its initial amplitude and phase at t_0 , respectively)

$$p_{\text{CW}}^{\text{fd}}(t) = A_{\text{CW}}^{t_0} \exp[i\sigma_{\text{CW}}(t - t_0) + i\alpha_{\text{CW}}^{t_0}] \tag{3}$$

and the excited part of PM through integration

$$p_{\text{obs}}^{\text{ext}}(t) = -i\sigma_{\text{CW}} \exp(i\sigma_{\text{CW}}t) \int_{t_0}^t \chi_{\text{obs}}(\tau) \exp(-i\sigma_{\text{CW}}\tau) d\tau \tag{4}$$

or through the time–frequency domain conversion (with numerical improvements from Chen et al., 2023, Optimal estimation of geodetic excitations from polar motion observations, manuscript in preparation)

$$\begin{aligned} p_{\text{obs}}^{\text{ext}}(t) &= \text{IFT}[p_{\text{obs}}^{\text{ext}}(f)], \\ p_{\text{obs}}^{\text{ext}}(f) &= \frac{\sigma_{\text{CW}}}{\sigma_{\text{CW}} - 2\pi f} \chi_{\text{obs}}(f) \\ &= \left[1 + \frac{2f}{F_{\text{CW}}(2 + i/Q_{\text{CW}}) - 2f} \right] \chi_{\text{obs}}(f). \end{aligned} \tag{5}$$

which will be respectively referred to as the “INT” and the “IFT” cases hereafter (INT is short for numerical integration while IFT denotes inverse Fourier transformation; IFT[x] means applying IFT to x). In Eqs. (2), (4) and (5), we have used the subscript “obs” to stress that $p_{\text{obs}}^{\text{ext}}(t)$ is excited by the observed excitation which is much more accurately determined than geophysical excitations (please refer to discussions in the Appendix and references therein).

Given initial values T_{CW}^0 and Q_{CW}^0 , $p_{\text{obs}}^{\text{ext}}(t)$ can be obtained either from Eq. (4) for the INT case or from Eq. (5) for the IFT case. Then, the time series for freely decaying CW may be obtained by

$$p_{\text{CW}}^{\text{fd}}(t) = p_{\text{obs}}(t) - p_{\text{obs}}^{\text{ext}}(t) \tag{6}$$

according to Eq. (2). The role of T_{CW} and Q_{CW} in the excitation of PM is obvious from Eqs. (1), (4), and (5). In Figs. 1 and 2, we present some examples of the observed PM, the excited part of PM, and the freely decaying part of the CW respectively derived from various PM data (more details can be found in Sects. 3 and 4).

On the other hand, by substituting Eq. (1) into Eq. (3), the freely decaying part of the CW can be written as (see also Gross 2015b)

$$p_{\text{CW}}^{\text{fd}}(t) = A_{\text{CW}}(t) \exp\left[i\left(\frac{2\pi}{T_{\text{CW}}}(t - t_0) + \alpha_{\text{CW}}^{t_0}\right)\right] \tag{7}$$

with the decaying amplitude

$$A_{\text{CW}}(t) = A_{\text{CW}}^{t_0} \exp\left[-\frac{\pi}{D_{\text{CW}}}(t - t_0)\right]. \tag{8}$$

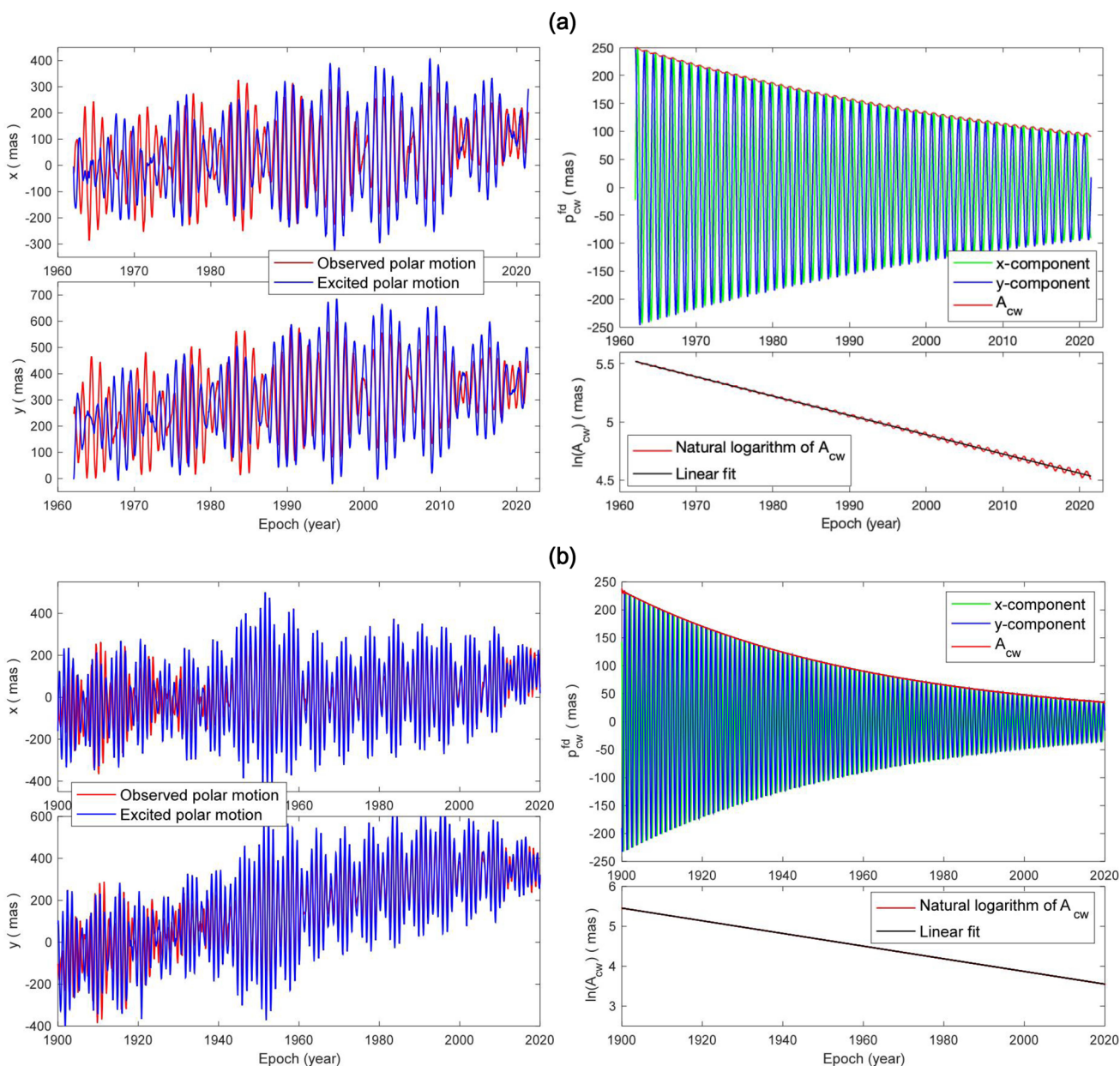


Fig. 1 The observed polar motion, the excited polar motion and freely decaying part of the Chandler wobble derived from the COMB2020 and POLE2020 PM series with selected values of T_{CW} and Q_{CW} . The corresponding amplitudes of the freely decaying Chandler wobble $A_{CW}(t)$ and the natural logarithm of $A_{CW}(t)$ are also provided. Here

$p_{obs}^{ext}(t)$ are derived from integration as defined by Eq. (4). Descriptions of the data series are given in Sect. 3. **a** COMB2020 with $T_{CW} = 427.4$ mean solar days and $Q_{CW} = 162$; **b** POLE2020 with $T_{CW} = 427.3$ mean solar days and $Q_{CW} = 159$

Taking the natural logarithm of Eq. (8), we get

$$\ln A_{CW}(t) = \ln A_{CW}^{t_0} - \frac{\pi}{D_{CW}}(t - t_0) \equiv K(t - t_0) + B, \tag{9}$$

$$K = -\frac{\pi}{D_{CW}}, \quad B = \ln A_{CW}^{t_0}$$

which implies $\ln A_{CW}(t)$ is a linear function of time t (Gross 2015b). Through the slope K , we will obtain $\hat{T}_{CW}(\equiv \hat{T}_{CW}^0 Q_{CW}^0) = -\pi / K$.

For self-consistent estimates of T_{CW} and Q_{CW} , \hat{D}_{CW} must equal $T_{CW}^0 Q_{CW}^0$. However, usually $\hat{D}_{CW} \neq T_{CW}^0 Q_{CW}^0$, thus giving rise to inconsistencies. Let us denote the difference as

$$v = \hat{D}_{CW} - T_{CW}^0 Q_{CW}^0. \tag{10}$$

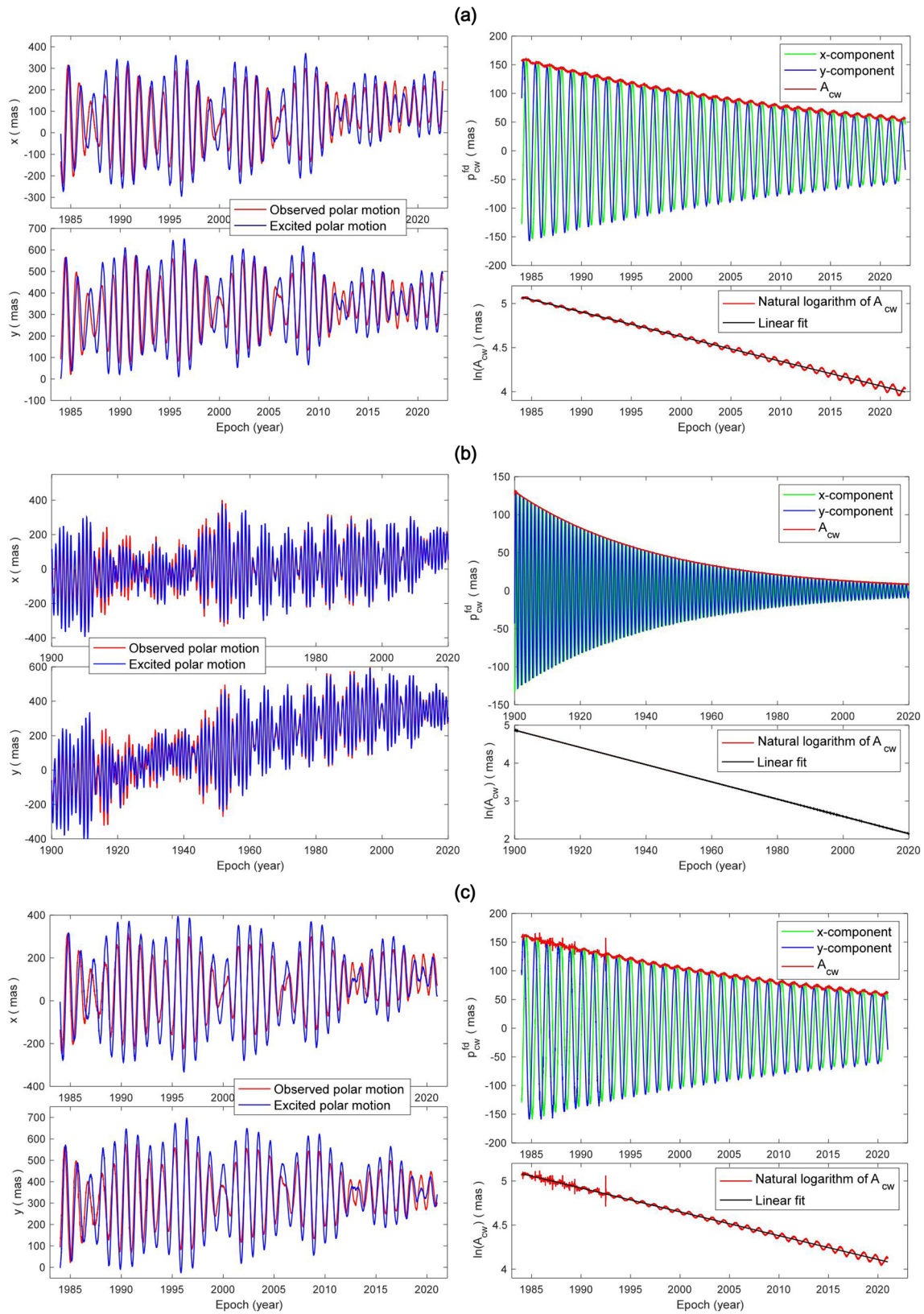


Fig. 2 Similar to Fig. 1, but for different PM series. **a** IERS 14 C04 with $T_{CW} = 432.7$ mean solar days and $Q_{CW} = 95$; **b** IERS C01 with $T_{CW} = 420.0$ mean solar days and $Q_{CW} = 120$; **c** ITRF2020 with $T_{CW} =$

428.9 mean solar days and $Q_{CW} = 99$ (the ITRF2020 PM series has been truncated as explained in Sect. 4.2)

Then, we seek the best inputs T_{CW}^0 and Q_{CW}^0 to let $|v| \rightarrow 0$, or numerically, $|v| \leq \varepsilon$ where ε is an arbitrarily small positive number. In this study, we adopt the traverse method to find the most self-consistent estimates.

3 Data

Due to the reasons explained in the Appendix and the method described in Sect. 2, only the observed PM data (expressed as $p(t) = x(t) - iy(t)$) are needed in this study. A number of EOP data (including PM time series) are available online or upon request. The EOP data adopted by us are listed below.

(1) PM from both the COMB2020 and POLE2020 EOP data (Gross et al. 1998; Ratcliff and Gross 2021) released by the Jet Propulsion Laboratory (JPL; available upon request to Dr. Richard Gross (richard.s.gross@jpl.nasa.gov); accessed on 8 Aug. 2022). By combining the individual Earth orientation series determined by lunar laser ranging (LLR), satellite laser ranging (SLR), very long baseline interferometry (VLBI), the global positioning system (GPS), and optical astrometric measurements using a Kalman filter, the COMB2020 and POLE2020 EOP series are expected to integrate unique strengths of each technique, which is sensitive to a different subset and/or linear combination of the EOPs. For both series, x and y are daily-sampled in 10^{-6} arcsecond (10^{-3} milli-arcsecond, mas), with their temporal rates in 10^{-6} arcsecond/day (10^{-3} mas/day). The COMB2020 data are daily-sampled and range from 20 January 1962 to 30 June 2021, while the POLE2020 data are monthly-sampled (30.4375-day) and range from 20 January 1900 to 22 June 2021.

(2) PM from both the IERS (International Earth Rotation and Reference Systems Service) C01 and original IERS 14 C04 (sampled at noon; Bizouard et al. 2019) released by the EOP Product Center (respectively available at https://datacenter.iers.org/data/latestVersion/EOP_C01_IAU2000_1900-now.txt and ftp://iers.obspm.fr/iers/eop/eopc04/eopc04.dX_dY.12h.84-now; both accessed on 4 Aug. 2022). The IERS EOP C01 is a long term EOP series (Vondrak et al. 1995) given at 0.05 year interval and range from 1900.00 to 2022.55. It is regularly recomputed to take advantage on one hand of the improvement of the various individual contributions and on the other hand of the refinement of the analysis procedures. The IERS EOP 14 C04 is daily-sampled from 1 January 1984 to 4 July 2022 and routinely provided by the IERS in consistency with the International Terrestrial Reference Frame 2014 (ITRF2014; Altamimi et al. 2016). The C04 data are derived from a combination of operational EOP series observed by

VLBI, Global Navigation Satellite System (GNSS), SLR, and Doppler Orbitography and Radiopositioning Integrated by Satellite (DORIS). In this study, we choose to use the original C04 solution sampled at UTC12:00 (Coordinated Universal Time) since the data values are the pole coordinates of the ITRF 2014 solution before 1 January 2015, while the common C04 version is an interpolation of the UTC12:00 version at UTC0:00 (Christian Bizouard, 2018, personal communication). For both C01 and C04, x and y are in arcsecond.

(3) PM from the ITRF2020 EOP files (Altamimi 2022) released by the Institut national de l'information géographique et forestière (IGN; available at https://itrf.ign.fr/ftp/pub/itrf/itrf2020/ITRF2020_EOP-F1.DAT; accessed on 5 Aug. 2022). The ITRF2020 is the latest realization of the International Terrestrial Reference System based on completely reprocessed time series of station positions and EOPs provided by the Technique Centers of VLBI, GNSS, SLR, and DORIS, as well as local ties at colocation sites (according to <https://itrf.ign.fr/en/solutions/itrf2020>). PM reflects the time-dependent coordinates of the Earth's reference pole (currently the Celestial Intermediate Pole) with respect to the ITRF. As a part of the ITRF2020 solutions, the ITRF2020 PM time series is certainly a good choice as it is the only PM combination series that is computed in a fully consistent and rigorous way with the terrestrial frame itself. In these data, x and y are daily-sampled in mas with their temporal rates in mas/day, and range from 26 November 1979 to 31 December 2020.

The PM series together with their errors from COMB2020, POLE2020, IERS 14 C04, IERS C01 and ITRF2020 are plotted in Fig. 3, from which one can see that PM errors are considerably larger at early years (before 1994).

The geodetic (or observed) excitations derived from these PM series through Eq. (21) are also provided in Fig. 4. One can see that the ITRF2020-based excitations have significant noise before ~ 1994 , which leads to unrealistic estimates $T_{CW} = 420.9$ mean solar days and $Q_{CW} = 70$. This is because the ITRF series is based purely on observational data and the continuously observed GNSS input series only began in 1994, while COMB2020, POLE2020, IERS 14 C04 and IERS C01 use filter methods to smooth and interpolate the raw input PM values. Therefore, either filtering or truncation is needed for the ITRF2020 PM data to obtain reliable results (see Table 2). In this study, we prefer the estimates from truncated rather than filtered ITRF2020 PM series as filtering brings somewhat artificial features to the results (for example, the choice of passband and stopband frequencies is empirical and may lead to discrepancies that are difficult to track down).

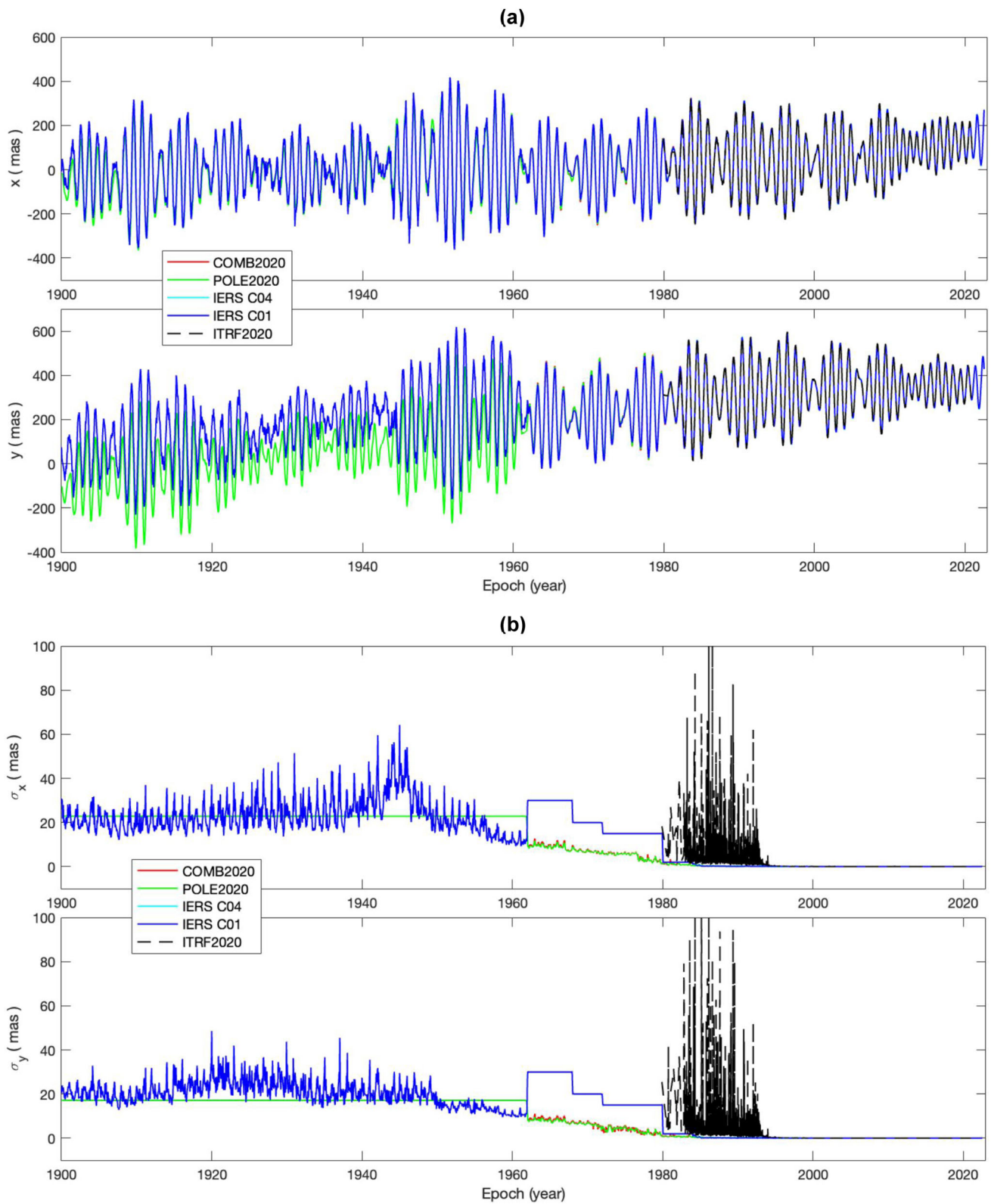


Fig. 3 Comparisons of the COMB2020, POLE2020, IERS 14 C04, IERS C01 and ITRF2020 polar motion series (a) and their reported errors (b)

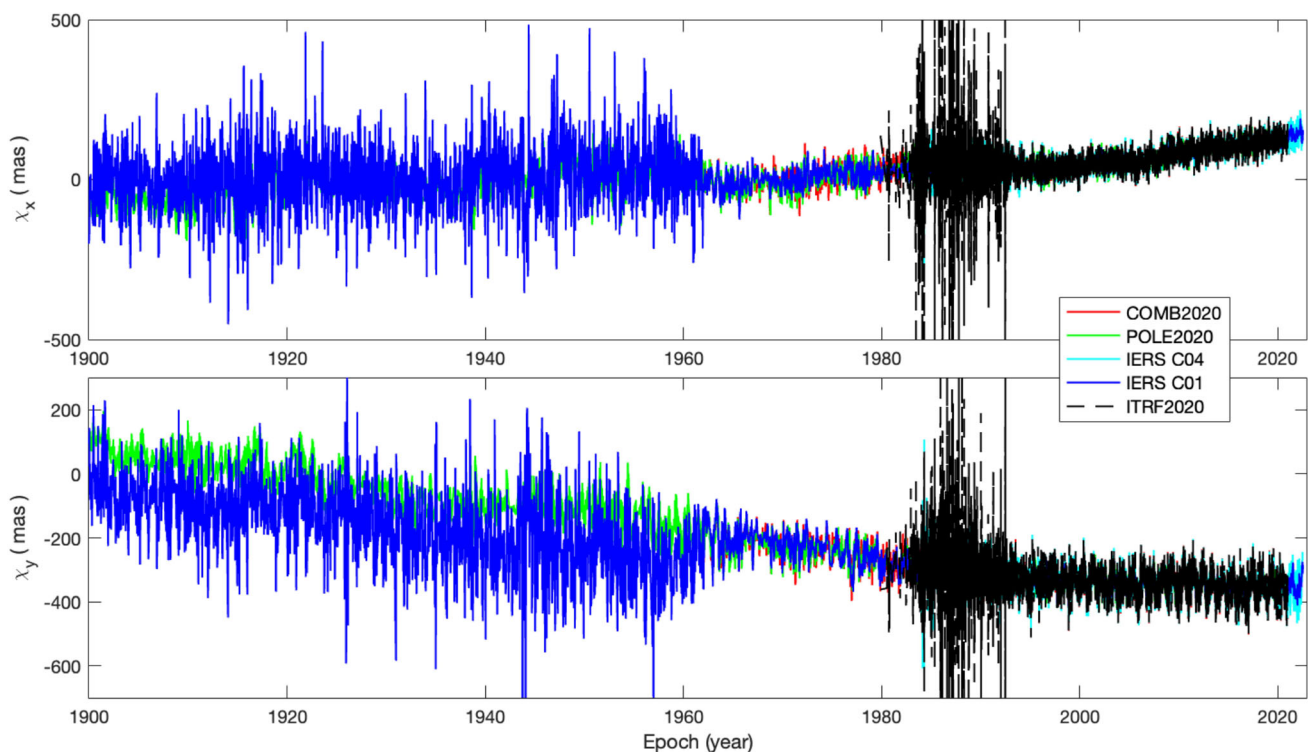


Fig. 4 Geodetic excitations derived from the COMB2020, POLE2020, IERS 14 C04, IERS C01 and ITRF2020 polar motion series

4 Numerical results

4.1 Preliminary results

The traverse algorithm (e.g., Hunt 2019) predicts a set of outcomes based on a range of values versus a set of fixed input values. Every input will be evaluated and thus traverse is able to find the globally optimal. Although it is less efficient, traverse is necessary to solve the current problem that has multiple local extremes (see below).

Relying on the method as described in Sect. 2, we have used T_{CW} ranging from 420 to 450 days with a 0.1-day step, and Q_{CW} ranging from 20 to 200 with a unit step to obtain v as defined by Eq. (10). That is, $301 \times 181 = 54,481$ trials for each simulation and thus 762,734 trials for all the 14 simulations (as listed in Table 2) are applied to find the best estimates. The results are illustrated by Fig. 5 (for clarity, the natural logarithm has been applied to $1/|v|$; only the case of IERS 14 C04 is shown) as well as Tables 1 and 2. One can see there are a number of local extremes lying between ~ 420 to ~ 447 days, which is not unexpected as these equations obviously set up a highly nonlinear problem. Therefore, one must be careful to make sure not to drop in these local extremes when estimating T_{CW} and Q_{CW} .

It is worth pointing out that many previous studies adopted the Monte Carlo Simulation to assign uncertainty intervals to T_{CW} and Q_{CW} , with white noises of some level added (e.g.,

Kuehne et al. 1996; Wilson and Chen 2005; Nastula and Gross 2015). Their uncertainty intervals may be related with the assumed level of white noises, while the uncertainties provided below should be more objective.

From Table 2, one can see T_{CW} and Q_{CW} estimates may vary with EOP series and methods (INT or IFT) adopted. They also vary with time span even for the same EOP series, which will be discussed in the next subsection. In fact, we have also used the famous digital filter developed by Wilson (1985), and found the results agree extremely closely with (almost exactly the same as) those listed in Table 2. The reasons may be: 1. the Wilson filter is accurate at the Chandler frequency and thus produces exactly the same outputs as Eq. (21) does at this frequency (valid for both the INT and IFT cases); 2. the accumulated errors of numerical integration are so large that the differences between the Wilson filter and Eq. (21) become unimportant (for the INT case only). In addition, T_{CW} and Q_{CW} estimates also vary with time span even for the same EOP series according to Table 2. These aspects are to be discussed in detail in the next subsection.

Obviously, the discrepancies in T_{CW} and Q_{CW} estimates reflect the errors introduced by the measurements and the numerical methods adopted to process the measured data. All the EOP series have provided formal errors, thus it seems possible to obtain the best estimates by weighted averaging of the preferred values (in bold) as listed in Table 2. However, the standard derivations of these errors in the given time

Fig. 5 Values of $\ln(1/|v|)$ in the traversal search (for the INT case of IERS 14 C04 EOP). **a** The 3D view; **b** The 2D contour. The maximum is marked in both figures

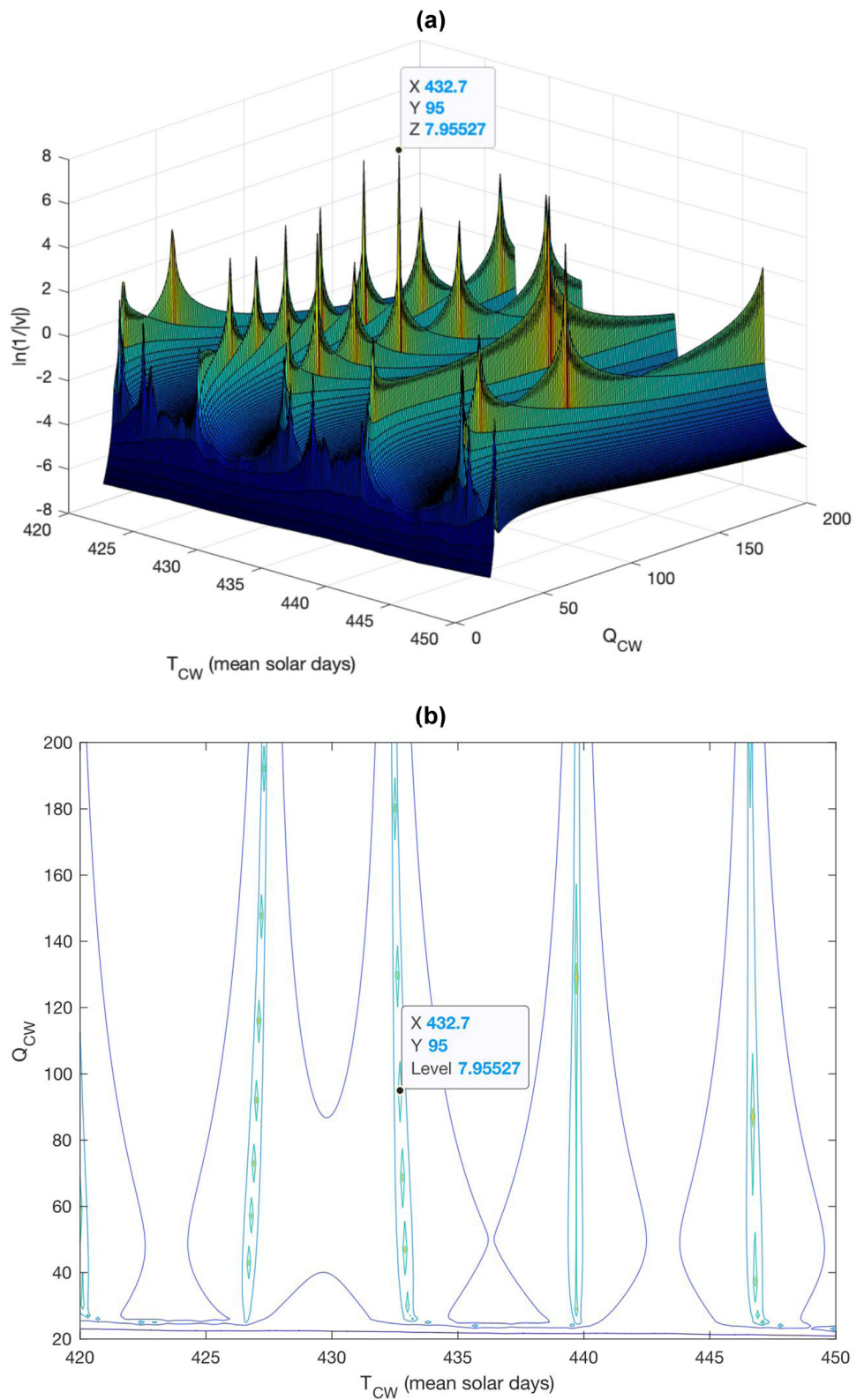


Table 1 Local extreme values of $\ln(1/|v|)$ and $|v|$ corresponding to Fig. 5 (only cases with $\ln(1/|v|)$ values > 5 are listed; preferred estimates are marked with bold numbers)

T_{CW}	Q_{CW}	$\ln(1/ v)$	$ v $
427.1	116	5.99989	0.002479
432.7	95	7.95527	0.000351
432.9	47	5.51115	0.004041
439.7	129	6.09516	0.002254
446.7	87	6.23023	0.001969

Table 2 Values of T_{CW} and Q_{CW} derived from different EOP time series for both the INT and IFT cases (for the two T_{CW} values for each simulation, the first one is in mean solar days and the other is in sidereal days; preferred estimates are marked with bold numbers)

EOP data	Time span	T_{CW} (INT)	Q_{CW} (INT)	T_{CW} (IFT)	Q_{CW} (IFT)		
COMB2020	1962.1.20–2021.6.30	427.4	428.6	162	433.6 ^a	434.8 ^a	166 ^a
COMB2020 ^b	1984.1.1–2020.12.31	428.3	429.5	198	430.1	431.3	155
POLE2020	1900.1.20–2021.6.22	427.3	428.5	159	432.9 ^a	434.1 ^a	167 ^a
IERS 14 C04	1984.1.1–2022.7.4	432.7	433.9	95	430.2	431.4	109
IERS C01	1900.00–2022.55	420.0	421.1	120	420.1	421.3	86
ITRF2020 EOP ^c	1979.11.26–2020.12.31	431.6	432.8	75	436.3	437.5	100
ITRF2020 EOP ^b	1984.1.1–2020.12.31	428.9	430.1	99	430.9	432.1	127

^a T_{CW} and Q_{CW} estimates are in fact unstable if too many data points before 1994 are used (see Sect. 4.2); these values appear to agree well with the others but in fact this is only coincidental

^bThese values are obtained from truncated EOP series in the time span 1 Jan. 1984 to 31 Dec. 2020

^cThese values are obtained by removing high-frequency noise in ITRF2020 PM; for the original ITRF2020 PM data, $T_{CW} = 420.9$ mean solar days or 422.1 sidereal days, and $Q_{CW} = 70$

spans, as listed in Table 2, are respectively

$$\sigma_{\text{COMB2020}} = 0.1555 \text{ mas,}$$

$$\sigma_{\text{IERS_C04}} = 0.2145 \text{ mas, and}$$

$$\sigma_{\text{ITRF2020}} = 6.4780 \text{ mas,}$$

according to the COMB2020, IERS 14 C04 and ITRF2020 EOP data (also see Fig. 3b for their error time series). The large σ values for ITRF2020 may indicate that its errors are closer to the true errors of the PM measurements, while the small σ values for the other series may be too optimistic, depending on how the individual PM series were combined. In other words, these σ values may not be of the same type, and thus it is not suitable to obtain the weighted average of the corresponding estimates relying on them. In view of this reason and the preferred estimates, we decide to use their arithmetic averages as the best estimates of CW parameters, which are respectively

For INT : $T_{CW} = 430.0 \pm 2.7$ mean solar days/431.1 \pm 2.8 sidereal days, and

$$Q_{CW} = 131 \pm 67,$$

and

For IFT : $T_{CW} = 430.4 \pm 0.5$ mean solar days/431.6 \pm 0.5

sidereal days, and

$$Q_{CW} = 130 \pm 25,$$

where we have taken $\max|T_{CW_X} - T_{CW}|$ and $\max|Q_{CW_X} - Q_{CW}|$ as the estimate errors ($X = \text{COMB2020, IERS 14 C04}$ or ITRF2020). The above INT and IFT results agree with each other quite well, indicating that our results are reliable. As the preferred results for the IFT case are obviously less scattered than those for the INT case, we would recommend the estimates from the IFT case as the best ones. The recommended estimates are generally in good agreement with results obtained by previous studies, though many of those are not self-consistent as explained in the Introduction as well as the Conclusion and Discussions (see also Sect. 5 for some equations underlying these discussions).

4.2 Longer time series, better results?

It is usually assumed that longer PM series will lead to better estimates of CW parameters. However, the numerical results as listed in Table 2 do not imply so. How come? We think the inhomogeneous errors and discontinuities in the long-term PM data are probably responsible.

To illustrate this, we have presented in Table 3 the estimates corresponding to three different periods for the same EOP series COMB2020: the first one with an 18.6 year (~

Table 3 Effect of data length on the estimates of Chandler parameters for both the INT and IFT cases (the COMB2020 series is adopted)

Time span	T_{CW} (INT)	Q_{CW} (INT)	T_{CW} (IFT)	Q_{CW} (IFT)		
2002.11.2–2021.6.30	432.0	433.2	127	430.1	431.3	120
1984.4.18–2021.6.30	430.3	431.5	164	428.7	429.9	117
1965.9.11–2021.6.30	425.8	427.0	111	438.6	439.8	48

6794 days) length, the second with a 37.2 (= 2*18.6) year length, and the third with a 55.8 (= 3*18.6) year length.

As pointed out in another study of ours (Luo et al. 2022), “if the Earth is a body with fixed size, figure and density distribution, the CW frequency, as a normal mode or eigenfrequency of the Earth, would be a constant. However, as is well known, the Earth is undergoing continuous deformations (namely changing figure and density distribution) due to loading and tidal attractions, etc.” There may be notable changes in T_{CW} due to tidal deformations caused by the largest, 18.6-year lunar tide, though for most loading and tidal deformations, the amount of figure changes and mass redistributions may not cause detectable T_{CW} variations. The choice of multiples of 18.6 years (as in Table 3) may help to avoid the possible influence of the 18.6-year tide on the estimates of T_{CW} .

One can see from Table 3 that, the 18.6-year and 37.2-year estimates are quite acceptable, while the T_{CW} value for the 55.8-year estimates is obviously somewhat biased for both the INT and IFT cases (Q_{CW} is also biased for the IFT case). We have also tried using POLE2020 and IERS C01 truncated into different time spans, but found T_{CW} estimates fluctuate between 420 ~ 450 days while Q_{CW} estimates fluctuate between 30 ~ 200, and no robust estimates can be obtained if too many data points at the early years are used. These are concrete examples supporting our argument that longer PM time series do not necessarily lead to better estimates of CW parameters, since early-year EOP data are of poor quality and can degrade the results.

For the INT case, the excited PM is calculated by numerical integration according to Eq. (4). During the course of numerical integration, the errors will accumulate into the integration results (the longer time span, the larger the error accumulated) and may bring the results far from the true values especially when the errors are large during the initial years. While recent PM errors are quite small (less than 0.05 mas), those in early years can be very large (over a few mas and can reach a few tens of mas; see Fig. 3b for errors for all PM series). The obvious discontinuities in PM and thus geodetic excitations (especially for IERS C01; see Figs. 3a and 4) also contribute to the integration errors.

For the IFT case, the excited PM is derived through time–frequency domain conversions. In the frequency domain, high-frequency noises are naturally separated from the frequencies near the Chandler band (thus T_{CW} and Q_{CW}

estimates are less affected by high-frequency noises), while in the time domain integration, high-frequency noises and real signals are mixed together, and thus errors will accumulate and become larger and larger when the time series are longer. Therefore, it is not unexpected that the preferred IFT estimates for COMB2000, IERS 14 C04 and ITRF2020 as listed in Table 2 are less scattered and all very close to the recommended values $T_{CW} = 430.4$ mean solar days and $Q_{CW} = 130$. Although the IFT method seems rather insensitive to high-frequency noises, it is sensitive to data discontinuities which lead to changes not only in trend but also in some low-frequency components (see Figs. 3a and 4, especially for IERS C01). While discontinuities are usually inevitable for very long time series, the IFT method can not be used to obtain reliable results either.

To conclude, for both the INT and IFT methods, longer PM time series do not necessarily lead to better results when taking into account the fact that PM data are of poor quality in the early years. Also, it is reasonable that we prefer the CW parameters estimated from truncated rather than full EOP series as discussed in Sect. 4.1.

5 Love numbers and PM transfer functions at chandler period

With self-consistent estimates of T_{CW} and Q_{CW} , we can obtain the degree-2 Love numbers and further PM transfer functions constrained by the CW parameters.

The theoretical expression for the Chandler wobble is (e.g., Mathews et al. 1991, 2002)

$$\sigma_{CW} = \frac{2\pi}{\Lambda} \frac{A}{A_m} (e - \kappa), \quad e = \frac{C - A}{A}, \quad \Lambda = \frac{\text{LOD}}{2\pi/\Omega} \quad (11)$$

where e and κ are respectively the dynamical ellipticity and compliance for the whole solid Earth, while A and A_m are respectively the equatorial principal moments of inertia of the whole solid Earth and the mantle, and $\text{LOD} = 86,400$ s is the nominal length of mean solar day. The compliance κ is closely related with the degree-2 tidal Love number k (e.g., Chen et al. 2013a):

$$\kappa = \frac{e}{k_s} k, \quad k_s = \frac{3G(C - A)}{\Omega^2 a^5} = \frac{3GAe}{\Omega^2 a^5}, \quad (12)$$

Table 4 Values of relevant parameters (uncertainties are provided in parentheses)

Parameter	Numeric value	Data source
$G (\times 10^{-11} \text{ m}^3 \text{ kg}^{-1} \text{ s}^{-2})$	6.67430(15)	CODATA2018
a (m)	6,378,136.6(1)	IERS Conventions (2010)
$e (\times 10^{-3})$	3.2845479(12)	Mathews et al. (2002)
$\Omega (\times 10^{-5} \text{ rad s}^{-1})$	7.292115	IERS Conventions (2010)
$A (\times 10^{37} \text{ kg m}^2)$	8.00804(18)	Updated from Chen et al. (2015)
$C (\times 10^{37} \text{ kg m}^2)$	8.03435(18)	Updated from Chen et al. (2015)
$A_m (\times 10^{37} \text{ kg m}^2)$	7.09675	Updated from Chen et al. (2015)
$C_m (\times 10^{37} \text{ kg m}^2)$	7.12065	Updated from Chen et al. (2015)
k_s	0.938324(89)	Derived by this study

where k_s is usually referred to as the secular Love number. Combining Eqs. (1), (11) and (12), the “CW parameter-constrained” complex tidal Love number reads (here T_{CW} should be in mean solar days; Λ must be replaced by 1 if T_{CW} is in sidereal days)

$$k = k_s \left[1 - \frac{A_m}{Ae} \frac{\Lambda}{T_{CW}} \left(1 + \frac{i}{2Q_{CW}} \right) \right], \quad \Lambda = \frac{\text{LOD}}{2\pi/\Omega} \quad (13)$$

Using $T_{CW} = 430.4$ mean solar days and $Q_{CW} = 130$, the k value is.

$$k = 0.35010616 - 0.00226238i$$

according to numerical values of relevant parameters consistent with the latest CODATA2018 (Committee on Data for Science and Technology 2018) numerical standards (Tiesinga et al. 2021; see Table 4). In Table 4, values of relevant parameters together with their uncertainties (if any) are provided. While Ω is the nominal mean Earth’s angular velocity without uncertainty, A_m and C_m are in fact modified from the values derived from the Preliminary Reference Earth Model (Dziewonski and Anderson 1981), which does not provide parameter uncertainties, and thus the uncertainties of A_m and C_m can not be determined (see Chen et al. (2015) for details). Uncertainties for all Love numbers discussed here (according to Eq. (13)) and thus for PM transfer functions are also unavailable. Although their values are assigned 8 decimal places, it does not mean they have such high accuracy. Users can truncate them according to their needs.

As shown in Chen et al. (2013a), the relation (let L denote a Love number of any type and ΔL be its increment due to

the Earth’s frequency-dependent responses)

$$\frac{\Delta k(f)}{k(f_R)} = \frac{\Delta h(f)}{h(f_R)} = \frac{\Delta l(f)}{l(f_R)} = \frac{\Delta k'(f)}{k'(f_R)} = \frac{\Delta h'(f)}{h'(f_R)} = \frac{\Delta l'(f)}{l'(f_R)} \quad (14)$$

holds at least from daily to decadal time scales. Wherein, h and l are tidal Love numbers respectively for vertical and horizontal displacements, while k' , h' and l' are the corresponding load Love numbers (we limit the case to degree-2 here). Choosing the reference frequency $f_R = 1$ cycle per day and using the nominal values of diurnal Love numbers as listed in Chapters 6 and 7 of the IERS Conventions (2010), the numerical values of these Love numbers, valid for the Chandler period, are

$$\begin{aligned} h &= 0.71101009 - 0.00459453i \\ l &= 0.09753209 - 0.00063025i \\ k' &= -0.36090393 + 0.00233215i \\ h' &= -1.17484499 + 0.00759182i \\ l' &= -0.15199044 + 0.00098216i \end{aligned}$$

The PM transfer functions T^L and T^{NL} (see Eq. (19)) play significant roles in understanding the relationship between polar motion and the underlying geophysical processes associated with mass redistributions and relative motions, and can be generally expressed as (e.g., Lambeck 1980; Dickman 2003; Chen et al. 2013a,b; Gross 2015a)

$$T_{PM}^{L/NL} = (1 + k')^\delta \frac{k_s}{k_s - k} \frac{A}{A_m}, \quad \delta = \begin{cases} 1 & \text{with loading} \\ 0 & \text{without loading} \end{cases} \quad (15)$$

where δ equals 1 or 0, depending on whether the concerning terms load the Earth or not (corresponding to the superscripts L and NL respectively). It is apparent that T^L and T^{NL} are determined by the Earth’s dynamic structure (A, A_m), (an)elasticity and rheology (k and k'), almost the same parameters determining the CW frequency as shown by Eqs. (11) and (12). Thus, the values of (T^L, T^{NL}) and (T_{CW}, Q_{CW}) are not independent but closely related to each other. This explains why in the Introduction we write “once the transfer functions are chosen, the values of T_{CW} and Q_{CW} are also fixed”.

The numerical values for PM transfer functions valid at the Chandler period are (these values are preferred by this study)

$$\begin{aligned} T^{NL} &= 1.80000957 - 0.00692311i \\ T^L &= 1.15039519 - 0.00022664i \end{aligned}$$

which are obviously different from $T^{\text{NL}} = \sim 1.62$ and $T^{\text{L}} = \sim 1.12$ (these two values are just those used by previous studies to estimate T_{CW} and Q_{CW}), valid around the diurnal period.

There are some disagreements on the existence of the factor A/A_{m} in the PM transfer functions (e.g., Dickman 2003; Chen et al. 2013a; Bizouard 2020). Below the values without the factor A/A_{m} are also provided:

$$T^{\text{NL}} = 1.59517423 - 0.00613529i$$

$$T^{\text{L}} = 1.01948389 - 0.00020085i$$

which are still different from the commonly adopted values $T^{\text{NL}} = \sim 1.62$ and $T^{\text{L}} = \sim 1.12$.

6 Conclusion and Discussions

The CW parameters (T_{CW} , Q_{CW}) and PM transfer functions (T^{NL} , T^{L}) reflect almost the same characteristics of the Earth, namely its layered structure, mass distribution, elasticity, rheology and energy dissipation, in different aspects, and thus they are not independent. Therefore, the CW parameters estimated from constant and real-valued transfer functions are not self-consistent. Recognizing this, we propose the use of $\chi_{\text{obs}}(t)$ (rather than the geophysical excitation $\chi_{\text{geo}}(t)$; see the ‘‘Appendix’’ for a brief discussion) to separate the observed PM into contributions from the freely decaying CW and the excited PM, and develop a self-consistent traverse-based method to search values of T_{CW} and Q_{CW} that can fit both parts simultaneously. It is worth noting that there are a number of local extremes and one must be careful to make sure not to drop in these local extremes when estimating T_{CW} and Q_{CW} . Our estimates $T_{\text{CW}} = 430.4 \pm 0.5$ mean solar days and $Q_{\text{CW}} = 130 \pm 25$ agree with the results obtained by previous studies, but are more self-consistent.

One should note that it is the errors of EOP measurements and the method adopted to derive geodetic excitation that give birth to the uncertainties of T_{CW} and Q_{CW} estimates. Most EOP data (such as COMB2020 and IERS 14 C04) only provide formal errors, which reflect the accuracy of data combinations and are usually smaller than true errors (One can refer to the errors provided by the ITRF2020 EOP, which are the most rigorously determined EOPs). In view of these points, we believe the differences of these EOP data are much closer to the true errors of EOP data, and thus our uncertainty intervals are directly obtained from the differences of (T_{CW} , Q_{CW}) estimated from three EOP series. Our uncertainties for T_{CW} and Q_{CW} may be more realistic than previous estimates.

Based on self-consistent estimates of T_{CW} and Q_{CW} , the degree-2 Love numbers and complex PM transfer functions valid at the Chandler period are provided in Sect. 4, among which the values of PM transfer functions are quite different

from the traditional transfer constants. However, even with previously accepted values $T_{\text{CW}} = 433$ mean solar days and $Q_{\text{CW}} = 100$, the Love numbers will be

$$k = 0.35203743 - 0.00293143i$$

$$k' = -0.36289477 + 0.00302184i$$

and PM transfer functions will be

$$T^{\text{NL}} = 1.80592052 - 0.00902960i$$

$$T^{\text{L}} = 1.15058869 - 0.00029560i$$

which are still quite different from the frequency-independent values $T^{\text{NL}} = \sim 1.62$ and $T^{\text{L}} = \sim 1.12$ used by previous studies (but consistent with the values provided by Chen et al. 2013a).

Recently, Liu et al. (2022) analyzed seasonal PM excitations in detail from both harmonic and inharmonic perspectives, and showed that the atmospheric, oceanic and hydrological excitations, constrained by satellite gravimetric measurements and with the frequency-dependent transfer functions of Chen et al. (2013a) applied, agree best with the geodetic excitation, while the unconstrained atmospheric, oceanic and hydrological excitations derived from general circulation models, with $T^{\text{NL}} = \sim 1.62$ and $T^{\text{L}} = \sim 1.12$ applied, have biased phases and smaller amplitudes compared to the geodetic excitation. Therefore, on one hand, geophysical excitations derived from general circulation models need further improvements and should be constrained by time-variable gravity observed by satellites; and on the other hand, the transfer functions developed by Chen et al. (2013a) and this study are reliable and can explain the geodetic excitation better provided that amplitudes and phases of global mass redistributions and relative motions are correctly modeled.

To conclude, the CW parameters as well as associated Love numbers and PM transfer functions derived by this study are reliable and acceptable, though further improvements are promising if accurate space geodetic EOP time series over longer time span are available, since the poor optical astrometric measurements in the early years can degrade these estimates.

Acknowledgements Dr. Richard S. Gross is highly appreciated for insightful discussions on estimating Chandler wobble quality factor through its free decay and for providing us the latest COMB2020, SPACE2020 and POLE2020 EOP data. Dr. Christian Bizouard is gratefully thanked for useful discussions on the IERS 14 C04 data. We also thank Prof. Michael Schindelegger, Dr. Christian Bizouard and two anonymous reviewers for insightful comments and suggestions which help to overcome some deficiencies in the original manuscript.

Funding This work is supported by the National Natural Science Foundation of China [grant numbers 41874025, 41474022].

Declarations

Conflict of Interest The authors declare no conflict of interest.

Open Access This article is licensed under a Creative Commons Attribution 4.0 International License, which permits use, sharing, adaptation, distribution and reproduction in any medium or format, as long as you give appropriate credit to the original author(s) and the source, provide a link to the Creative Commons licence, and indicate if changes were made. The images or other third party material in this article are included in the article's Creative Commons licence, unless indicated otherwise in a credit line to the material. If material is not included in the article's Creative Commons licence and your intended use is not permitted by statutory regulation or exceeds the permitted use, you will need to obtain permission directly from the copyright holder. To view a copy of this licence, visit <http://creativecommons.org/licenses/by/4.0/>.

Appendix: Liouville's Equation, Geophysical and Geodetic Excitations

Under the law of conservation of angular momentum, theoretical studies of polar motion are based on the application of the linearized Liouville equation for a rotationally stratified Earth (e.g., Gross 2015a)

$$\frac{i}{\sigma_{CW}} \frac{\partial p(t)}{\partial t} + p(t) = \chi(t), \quad i = \sqrt{-1}, \quad (16)$$

where $p(t) = x(t) - iy(t)$ the coordinates of the CIP measured in the ITRS, and $\chi(t)$ the excitation function (excitation for short hereafter) for polar motion.

As is well known, the time-domain solution to Eq. (16) can be written as

$$p_{\text{obs}}(t) = A_{CW}^{t_0} \exp[i\sigma_{CW}(t - t_0) + i\alpha_{CW}^{t_0}] - i\sigma_{CW} \exp(i\sigma_{CW}t) \int_{t_0}^t \chi(\tau) \exp(-i\sigma_{CW}\tau) d\tau, \quad (17)$$

where $p_{\text{obs}}(t)$ is the observed polar motion, and t_0 is the initial time. $\chi(t)$ is usually derived from data of mass redistributions $c(t)$ and relative motions $h(t)$ (such $\chi(t)$ are often called geophysical excitations, $\chi_{\text{geo}}(t)$). In order to take into account the Earth's frequency-dependent responses due to mantle anelasticity and viscoelasticity etc., we can evaluate $\chi(t)$ in the frequency domain (with Ω the nominal rotation rate of the Earth; e.g., Chen et al. 2013a,b, 2017):

$$\tilde{\chi}_{\text{geo}}(f) = T^L(f) \frac{\tilde{c}(f)}{C - A} + T^{NL}(f) \frac{\tilde{h}(f)}{\Omega(C - A)}, \quad (18)$$

and then apply the Inverse Fourier Transformation (IFT) to it, namely $\chi(t) = \text{IFT}[\tilde{\chi}(f)]$. In Eq. (18), the PM transfer functions T^L and T^{NL} (L and NL for with and without loading

effects, respectively) describe the responses of the stratified and deformable Earth (e.g., Lambeck 1980; Dickman 2003; Chen et al. 2013b, a; Gross 2015a).

The freely decaying part of the CW and the excited part of PM can thus be written as

$$p_{CW}^{\text{fd}}(t) = A_{CW}^{t_0} \exp[i\sigma_{CW}(t - t_0) + i\alpha_{CW}^{t_0}] \quad (19)$$

and

$$p^{\text{ext}}(t) = -i\sigma_{CW} \exp(i\sigma_{CW}t) \int_{t_0}^t \chi(\tau) \exp(-i\sigma_{CW}\tau) d\tau, \quad (20)$$

respectively. Obviously, $p^{\text{ext}}(t)$ can be obtained by a numerical integration once $\chi(t)$ is known. In this study we prefer to use $\chi(t)$ derived from the observed polar motion (often called observed excitation or geodetic excitation, $\chi_{\text{obs}}(t)$) rather than the geophysical excitation $\chi_{\text{geo}}(t)$. In the ideal case, $\chi_{\text{geo}}(t)$ should equal $\chi_{\text{obs}}(t)$, however there are notable differences between them due to the fact that mass redistributions and relative motions are not accurately modeled (e.g., Chen et al. 2013b; Harker et al. 2021; Liu et al. 2022) and it will take considerable extra efforts to improve $\chi_{\text{geo}}(t)$ (e.g., Göttl et al. 2012, 2015; Chen et al. 2017, 2019) to obtain reliable estimates of T_{CW} and Q_{CW} . Further, it is sufficient to use $\chi_{\text{obs}}(t)$ rather than $\chi_{\text{geo}}(t)$ here since this study does not discuss which geoprocess(es) contribute(s) the most to the excitations of CW.

In addition, we shall use a method based on the combined frequency and time-domain Liouville's equation (see e.g., Chen et al 2017; 2023), to derive $\chi(t)$. Applying the Fourier Transformation (FT) to Eq. (16), and letting $\chi_{\text{obs}}(f)$ and $p_{\text{obs}}(f)$ respectively be the frequency components of $\chi_{\text{obs}}(t)$ and $p_{\text{obs}}(t)$, one obtains

$$\begin{aligned} \chi_{\text{obs}}(f) &= \frac{\sigma_{CW} - 2\pi f}{\sigma_{CW}} p_{\text{obs}}(f) \\ &= \left[1 - \frac{2}{2 + i/Q_{CW}} \frac{f}{F_{CW}} \right] p_{\text{obs}}(f), \\ F_{CW} &= \frac{1}{T_{CW}}, \end{aligned} \quad (21)$$

and thus $\chi_{\text{obs}}(t)$ through the inverse Fourier transformation (IFT) of $\chi_{\text{obs}}(f)$. We then obtain the initial CW by replacing $\chi(t)$ in Eq. (6) with $\chi_{\text{obs}}(t)$. More details on how to use Eq. (21) to derive the geodetic excitation, together with some improvements to Eq. (21), are discussed in Chen et al. (2023, in preparation), where validations of this method are also presented.

References

1. Altamimi Z, Rebischung P, Métivier L, Collilieux X (2016) ITRF2014: a new release of the international terrestrial reference frame modeling nonlinear station motions. *J Geophys Res Solid Earth* 121:6109–6131. <https://doi.org/10.1002/2016JB013098>
2. Altamimi Z (2022) Description of the ITRF2020 solutions. Available online: <https://itrf.ign.fr/en/solutions/itrf2020>. Accessed 5 Aug 2022
3. Bizouard C (2020) Geophysical modelling of the polar motion. De Gruyter, Berlin. <https://doi.org/10.1515/9783110298093>
4. Bizouard C, Lambert S, Gattano C, Becker O, Richard JY (2019) The IERS EOP 14C04 solution for Earth orientation parameters consistent with ITRF 2014. *J Geod* 93:621–633
5. Brzezinski A, Nastula J (2002) Oceanic excitation of the Chandler wobble. *Adv Space Res* 30:195–200
6. Chen W, Ray J, Li JC, Huang CL, Shen WB (2013a) Polar motion excitations for an Earth model with frequency-dependent responses: 1. A refined theory with insight into the earth's rheology and core-mantle coupling. *J Geophys Res Solid Earth* 118:4975–4994. <https://doi.org/10.1002/jgrb.50314>
7. Chen W, Ray J, Shen WB, Huang CL (2013b) Polar motion excitations for an Earth model with frequency-dependent responses: 2. Numerical tests of the meteorological excitations. *J Geophys Res Solid Earth* 118:4995–5007
8. Chen W, Li JC, Ray J, Shen WB, Huang CL (2015) Consistent estimates of the dynamical figure parameters of the Earth. *J Geod* 89:179–188. <https://doi.org/10.1007/s00190-014-0768-y>
9. Chen W, Li JC, Ray J, Cheng MK (2017) Improved geophysical excitations constrained by polar motion observations and GRACE/SLR time-dependent gravity. *Geodesy Geodyn* 8:377–388. <https://doi.org/10.1016/j.geog.2017.04.006>
10. Chen W, Luo J, Ray J, Yu N, Li J (2019) Multiple-data-based monthly geopotential model set LDCmgm90. *Sci Data* 6:228. <https://doi.org/10.1038/s41597-019-0239-7>
11. Dickman SR (2003) Evaluation of “effective angular momentum function” formulations with respect to core-mantle coupling. *J Geophys Res* 108(B3):2150. <https://doi.org/10.1029/2001JB001603>
12. Dziewonski AM, Anderson DL (1981) Preliminary reference Earth model. *Phys Earth Planet Inter* 25:297–356. [https://doi.org/10.1016/0031-9201\(81\)90046-7](https://doi.org/10.1016/0031-9201(81)90046-7)
13. Furuya M, Chao BF (1996) Estimation of period and Q of the Chandler wobble. *Geophys J Int* 127(3):693–702
14. Göttl F, Schmidt M, Heinkelmann R, Savcenko R, Bouman J (2012) Combination of gravimetric and altimetric space observations for estimating oceanic polar motion excitations. *J Geophys Res* 117:C10022
15. Göttl F, Schmidt M, Seitz F, Bloßfeld M (2015) Separation of atmospheric, oceanic and hydrological polar motion excitation mechanisms based on a combination of geometric and gravimetric space observations. *J Geod* 89:377–390
16. Gross RS (2000) The excitation of the Chandler wobble. *Geophys Res Lett* 27(15):2329–2332
17. Gross RS, Eubanks TM, Steppe JA, Freedman AP, Dickey JO, Runge TF (1998) A Kalman-filter-based approach to combining independent Earth-orientation series. *J Geodesy* 72:215–235
18. Gross RS, Fukumori I, Menemenlis D (2003) Atmospheric and oceanic excitation of the Earth's wobbles during 1980–2000. *J Geophys Res* 108(B8):2370. <https://doi.org/10.1029/2002JB002143>
19. Gross RS (2015a) Earth rotation variations—long period. In: *Treatise on geophysics 2nd edn vol 3* (ed. Schubert, G.) Ch.9 (Elsevier B. V., 2015a)
20. Gross RS (2015b) Estimating the Q of the Chandler wobble from its free decay. AGU Fall Meeting, Abstract No.G11A-0966
21. Harker AA, Schindelegger M, Ponte RM, Salstein DA (2021) Modeling ocean-induced rapid Earth rotation variations: an update. *J Geodesy* 95:110
22. Hunt J (2019) *Advanced guide to python 3 programming*. Springer, <https://doi.org/10.1007/978-3-030-25943-3>
23. IERS conventions (2010) In: Petit G, Luzum B (eds) *IERS Technical Notes 36*, Frankfurt am Main: Verlag des Bundesamts für Kartographie und Geodäsie, ISBN 3–89888–989–6 (2010).
24. Jeffreys H (1972) The variation of latitude. In: Melchior P, Yumi S (eds) *Rotation of the Earth*, Int. Astron. Union Symp. No. 48, pp 39–42. D. Reidel, Dordrecht, Holland
25. Kuehne J, Wilson CR, Johnson S (1996) Estimates of the Chandler wobble frequency and Q. *J Geophys Res* 101(B6):13573–13579
26. Lambeck K (1980) *The earth's variable rotation: geophysical causes and consequences*. Cambridge University Press, Cambridge
27. Liu H, Zhou Y, Ray J, Luo J (2022) Excitations of seasonal polar motions derived from satellite gravimetry and general circulation models: comparisons of harmonic and inharmonic analyses. *Remote Sens* 14:3567. <https://doi.org/10.3390/rs14153567>
28. Luo J, Chen W, Ray J, Li J (2022) Short-term polar motion forecast based on the holt-winters algorithm and angular momenta of global surficial geophysical fluids. *Surv Geophys*. <https://doi.org/10.1007/s10712-022-09733-0>
29. Mathews PM, Buffett BA, Herring TA, Shapiro II (1991) Forced nutations of the Earth: Influence of inner core dynamics: 1. Theory. *J Geophys Res* 96:8219–8242. <https://doi.org/10.1029/90JB01955>
30. Mathews PM, Herring TA, Buffett BA (2002) Modeling of nutation and precession: New nutation series for nonrigid Earth and insights into the Earth's interior. *J Geophys Res* 107(B4):2068. <https://doi.org/10.1029/2001JB000390>
31. Nastula J, Gross R (2015) Chandler wobble parameters from SLR and GRACE. *J Geophys Res Solid Earth* 120(6):4474–4483
32. Ooe M (1978) An optimal complex AR-MA model of the Chandler wobble. *Geophys J Int* 53(3):445–457
33. Ratcliff JT, Gross RS (2021) Combinations of earth orientation measurements: SPACE2020, COMB2020, and POLE2020. NASA Report number: JPL 21–1
34. Seitz F, Kirschner S, Neubersch D (2012) Determination of the Earth's pole tide Love number k₂ from observations of polar motion using an adaptive Kalman filter approach. *J Geophys Res Solid Earth* 117(B9).
35. Tiesinga E, Mohr P, Newell D, Taylor B (2021) CODATA recommended values of the fundamental physical constants: 2018. *Rev Mod Phys* 93:025010
36. Vondrak J, Ron C, Pesek I, Cepek A (1995) New global solution of earth orientation parameters from optical astrometry in 1900–1990. *Astron Astrophys* 297:899–906
37. Wilson CR (1985) Discrete polar motion equations. *Geophys J R Astron Soc* 80:551–554
38. Wilson CR, Haubrich RA (1976) Meteorological excitation of the Earth's wobble. *Geophys J Roy Astron Soc* 46:707–743
39. Wilson CR, Vicente RO (1980) An analysis of the homogeneous ILS polar motion series. *Geophys J Roy Astron Soc* 62:605–616
40. Wilson CR, Chen J (2005) Estimating the period and Q of the Chandler wobble. In: Plag HP, Chao BF, Gross RS, and van Dam T (eds) *Forcing of polar motion in the chandler frequency band: a contribution to understanding interannual climate change*, vol 24, pp 23–29
41. Wilson CR and Vicente RO (1990) Maximum likelihood estimates of polar motion parameters. In: McCarthy DD and Carter WE (eds.) *Variations in Earth Rotation*. American Geophysical Union Geophysical Monograph Series, vol. 59, pp. 151–155. Washington, DC: American Geophysical Union.